

**Supplementary Table 1. Data collection, phasing and refinement statistics**

|   | Native                           | ATP $\gamma$ S-Mg                | ADP-Mg-F                         | AMPPNP-Mn                        | Au                               | U                                |
|---|----------------------------------|----------------------------------|----------------------------------|----------------------------------|----------------------------------|----------------------------------|
| <b>Data collection</b>                              |                                  |                                  |                                  |                                  |                                  |                                  |
| Space group   | P2 <sub>1</sub> 2 <sub>1</sub> 2 | P2 <sub>1</sub> 2 <sub>1</sub> 2 | P2 <sub>1</sub> 2 <sub>1</sub> 2 | P2 <sub>1</sub> 2 <sub>1</sub> 2 | P2 <sub>1</sub> 2 <sub>1</sub> 2 | P2 <sub>1</sub> 2 <sub>1</sub> 2 |
| Cell dimensions                                     |                                  |                                  |                                  |                                  |                                  |                                  |
| <i>a, b, c</i> (Å)                                  | 163.2,<br>207.8,<br>139.4        | 162.8,<br>203.7,<br>138.7        | 163.8,<br>208.5,<br>138.5        | 162.9,<br>207.2,<br>140.0        | 163.3,<br>209.2,<br>139.7        | 162.8,<br>207.6,<br>139.0        |
| $\alpha, \beta, \gamma$ (°)                         | 90, 90, 90                       | 90, 90, 90                       | 90, 90, 90                       | 90, 90, 90                       | 90, 90, 90                       | 90, 90, 90                       |
| Resolution (Å)                                      | 30.0-3.2<br>(3.31-3.2)*          | 100.0-3.3<br>(3.42-3.3)          | 100.0-3.5<br>(3.63-3.5)          | 100.0-3.7<br>(3.83-3.7)          | 35.0-4.1<br>(4.25-4.1)           | 30.0-4.0<br>(4.14-4.0)           |
| <i>R</i> <sub>sym</sub>                             | 0.107<br>(0.538)                 | 0.149<br>(0.612)                 | 0.185<br>(0.665)                 | 0.178<br>(0.642)                 | 0.197<br>(0.615)                 | 0.186<br>(0.704)                 |
| <i>I</i> / $\sigma$ <i>I</i>                        | 11.3<br>(1.8)                    | 7.8<br>(1.4)                     | 5.9<br>(1.4)                     | 11.7<br>(2.3)                    | 9.2<br>(2.8)                     | 9.6<br>(2.3)                     |
| Completeness (%)                                    | 95.8<br>(79.4)                   | 98.5<br>(95.3)                   | 94.6<br>(83.6)                   | 99.6<br>(98.1)                   | 98.4<br>(99.1)                   | 88.9<br>(89.1)                   |
| Redundancy  | 3.7<br>(2.3)                     | 4.4<br>(2.5)                     | 3.6<br>(2.4)                     | 6.4<br>(5.5)                     | 6.6<br>(6.4)                     | 6.2<br>(5.6)                     |
| <b>Refinement</b>                                   |                                  |                                  |                                  |                                  |                                  |                                  |
| Resolution (Å)                                      | 30.0 – 3.2                       | 100.0 – 3.3                      | 100.0 – 3.5                      |                                  |                                  |                                  |
| No. reflections                                     | 66653                            | 63147                            | 49387                            |                                  |                                  |                                  |
| <i>R</i> <sub>work</sub> / <i>R</i> <sub>free</sub> | 22.2 / 25.6                      | 23.3 / 26.8                      | 23.1 / 25.1                      |                                  |                                  |                                  |
| No. atoms   |                                  |                                  |                                  |                                  |                                  |                                  |
| Protein   | 22126                            | 22126                            | 22126                            |                                  |                                  |                                  |
| Ligand  | 0                                | 66                               | 66                               |                                  |                                  |                                  |
| B-factors   |                                  |                                  |                                  |                                  |                                  |                                  |
| Protein   | 77.2                             | 70.8                             | 74.5                             |                                  |                                  |                                  |
| Ligand/ion  | -                                | 64.4                             | 64.3                             |                                  |                                  |                                  |
| R.m.s deviations                                    |                                  |                                  |                                  |                                  |                                  |                                  |
| Bond lengths (Å)                                    | 0.009                            | 0.007                            | 0.006                            |                                  |                                  |                                  |
| Bond angles (°)                                     | 1.418                            | 1.253                            | 1.133                            |                                  |                                  |                                  |

\*Highest resolution shell is shown in parenthesis.

**Supplementary Table 2. Superpositions of mTOR and PI3K kinase domains (rmsd in C $\alpha$  positions in Å)**

| Kinase domain             | mTOR | PI3K C3       | p110 $\alpha$ | p110 $\beta$ | p110 $\gamma$ | p110 $\delta$ |
|---------------------------|------|---------------|---------------|--------------|---------------|---------------|
| mTOR<br>(493)*            | -    | 1.7<br>(252)# | 1.9<br>(256)  | 1.7<br>(221) | 1.7<br>(249)  | 1.8<br>(243)  |
| PI3K C3 (3IHY)†           |      |               | 1.8<br>(289)  | 1.6<br>(291) | 1.8<br>(294)  | 1.4<br>(292)  |
| PI3K p110 $\alpha$ (2RDO) |      |               |               | 1.6<br>(310) | 1.7<br>(288)  | 1.4<br>(299)  |
| PI3K p110 $\beta$ (2Y3A)  |      |               |               |              | 1.5<br>(288)  | 1.1<br>(332)  |
| PI3K p110 $\gamma$ (1E8X) |      |               |               |              |               | 1.5<br>(288)  |
| PI3K p110 $\delta$ (2WXF) |      |               |               |              |               | -             |

\*Number of ordered residues in the structure of the specified kinase domain.

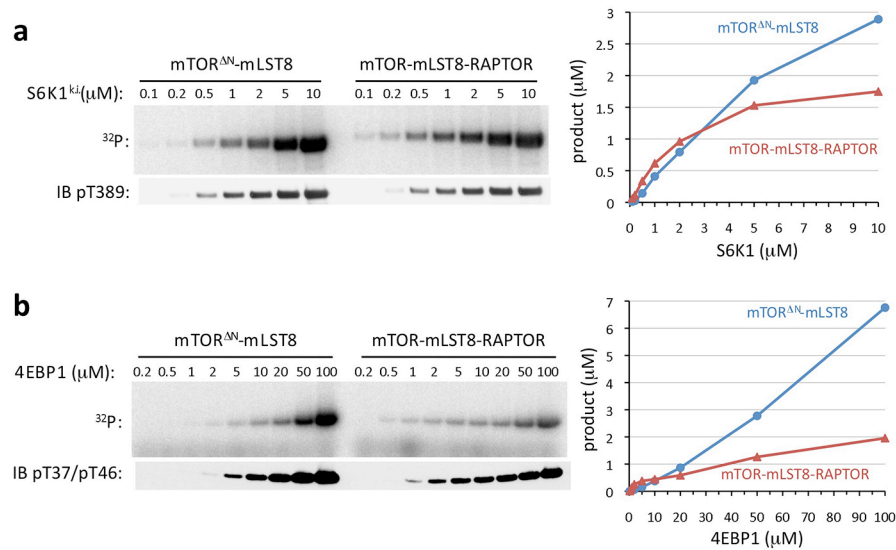
#Number of residues that superimpose at the indicated r.m.s.d.

†PDB id.

**Supplementary Table 3. Inhibitor data collection and refinement statistics**

|                                       | Torin2                           | PP242                            | PI-103                           |
|---------------------------------------|----------------------------------|----------------------------------|----------------------------------|
| <b>Data collection</b>                |                                  |                                  |                                  |
| Space group                           | P2 <sub>1</sub> 2 <sub>1</sub> 2 | P2 <sub>1</sub> 2 <sub>1</sub> 2 | P2 <sub>1</sub> 2 <sub>1</sub> 2 |
| Cell dimensions                       |                                  |                                  |                                  |
| <i>a, b, c</i> (Å)                    | 164.3,<br>208.3,<br>138.8        | 163.8,<br>207.0,<br>139.3        | 163.6,<br>207.7,<br>138.3        |
| $\alpha, \beta, \gamma$ (°)           | 90, 90, 90                       | 90, 90, 90                       | 90, 90, 90                       |
| Resolution (Å)                        | 40.0-3.55<br>(3.68-3.55)*        | 40.0-3.45<br>(3.57-3.45)         | 40.0-3.6<br>(3.73-3.60)          |
| R <sub>sym</sub>                      | 0.187<br>(0.669)                 | 0.176<br>(0.629)                 | 0.226<br>(0.650)                 |
| I/ $\sigma$ I                         | 7.3<br>(1.7)                     | 5.8<br>(1.3)                     | 4.7<br>(1.5)                     |
| Completeness (%)                      | 95.6<br>(71.1)                   | 97.0<br>(91.2)                   | 89.0<br>(76.9)                   |
| Redundancy                            | 3.5<br>(2.0)                     | 3.8<br>(2.7)                     | 3.3<br>(2.5)                     |
| <b>Refinement</b>                     |                                  |                                  |                                  |
| Resolution (Å)                        | 40.0 – 3.5                       | 40.0 – 3.45                      | 40.0 – 3.6                       |
| No. reflections                       | 49412                            | 52634                            | 40902                            |
| R <sub>work</sub> / R <sub>free</sub> | 22.8 / 25.9                      | 23.5 / 27.1                      | 24.0 / 27.5                      |
| No. atoms                             |                                  |                                  |                                  |
| Protein                               | 22126                            | 22126                            | 22126                            |
| Inhibitor                             | 64                               | 46                               | 52                               |
| B-factors                             |                                  |                                  |                                  |
| Protein                               | 76.1                             | 68.9                             | 65.7                             |
| Ligand/ion                            | 34.3                             | 36.1                             | 30.1                             |
| R.m.s deviations                      |                                  |                                  |                                  |
| Bond lengths (Å)                      | 0.007                            | 0.007                            | 0.006                            |
| Bond angles (°)                       | 1.279                            | 1.277                            | 1.219                            |

\*Highest resolution shell is shown in parenthesis.

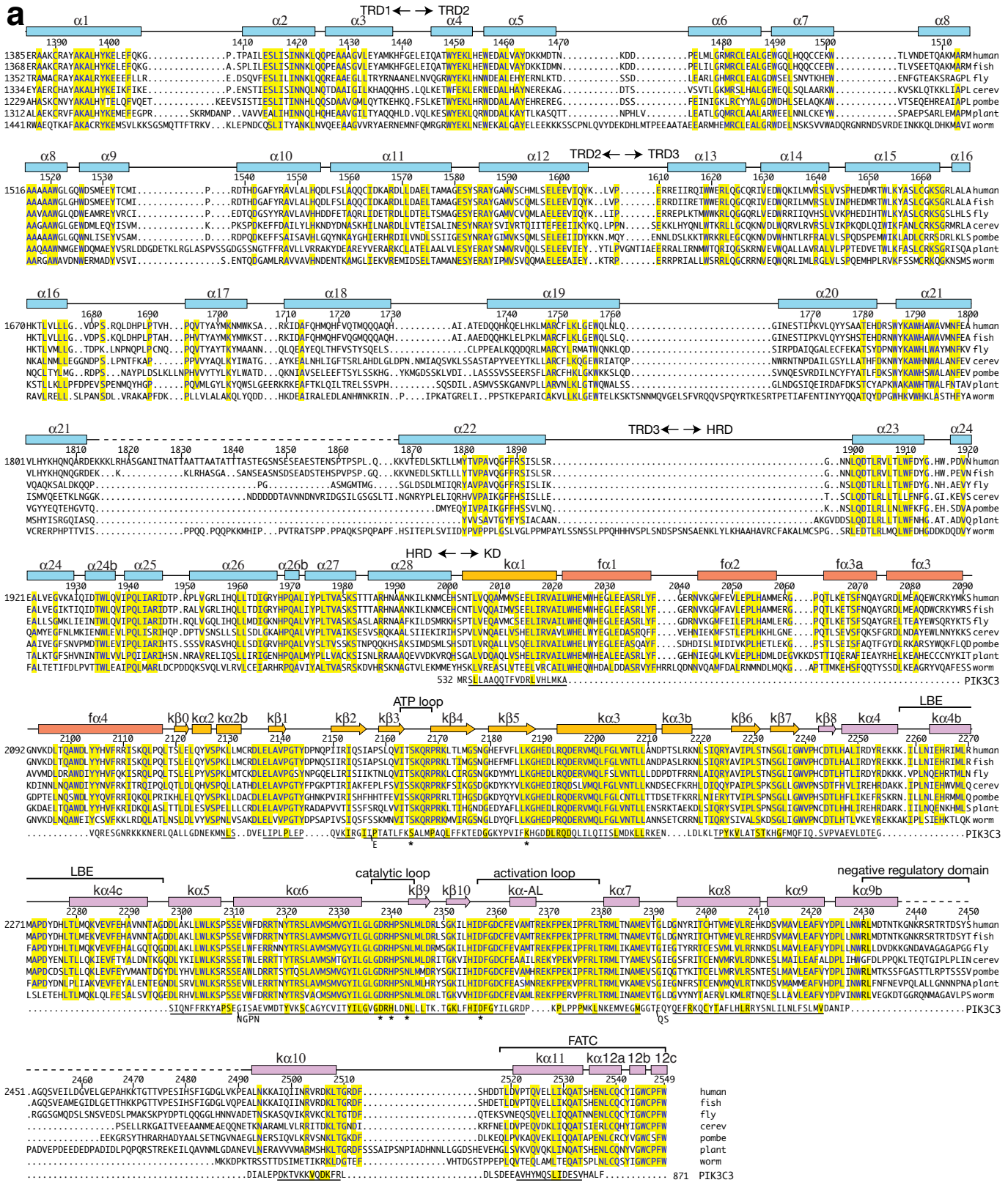


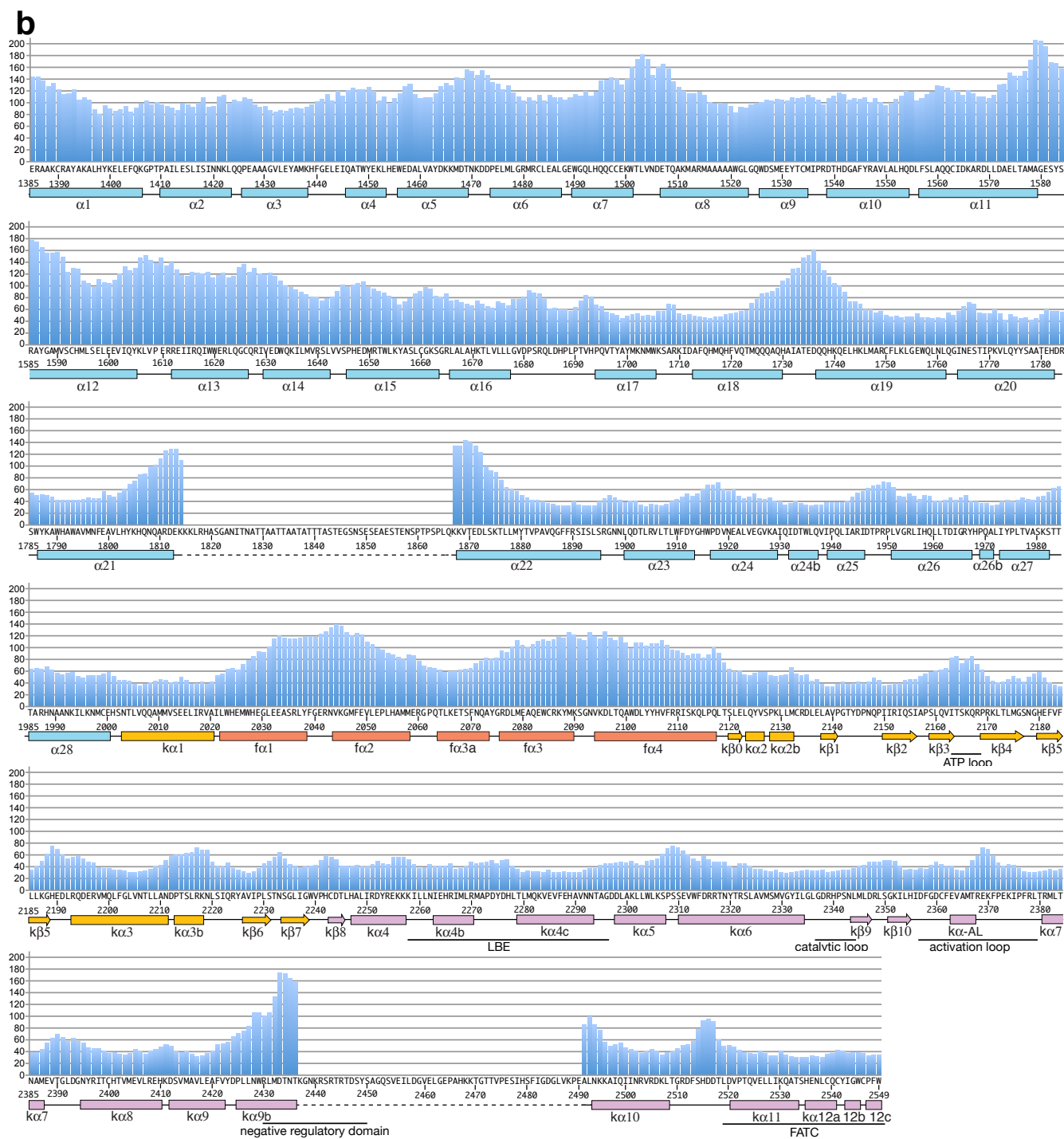
**Supplementary Figure 1. Phosphorylation of S6K1 and 4EBP1 by the mTOR<sup>ΔN</sup>-mLST8 and mTORC1 complexes.**

**a**, Phosphorylation of the indicated concentrations of full-length S6K1 harboring a kinase inactivating mutation (K100R, thereafter S6K1<sup>ki</sup>) by mTOR<sup>ΔN</sup>-mLST8 and mTORC1 (each at 100 nM concentration). Top panels are <sup>32</sup>P autoradiograms and lower panels are immunoblots using an S6K1 phosphoThr389-specific antibody. Reactions were performed as described in methods. Graph shows quantitation of the <sup>32</sup>P autoradiograms (blue circles for mTOR<sup>ΔN</sup>-mLST8, and red triangles for mTORC1).

**b**, Phosphorylation of the indicated concentrations of full-length 4EBP1 by mTOR<sup>ΔN</sup>-mLST8 and mTORC1. Assays were performed as in (a), except for immunoblotting with an antibody specific for 4EBP1 phosphorylated at Thr37 and Thr46.

a





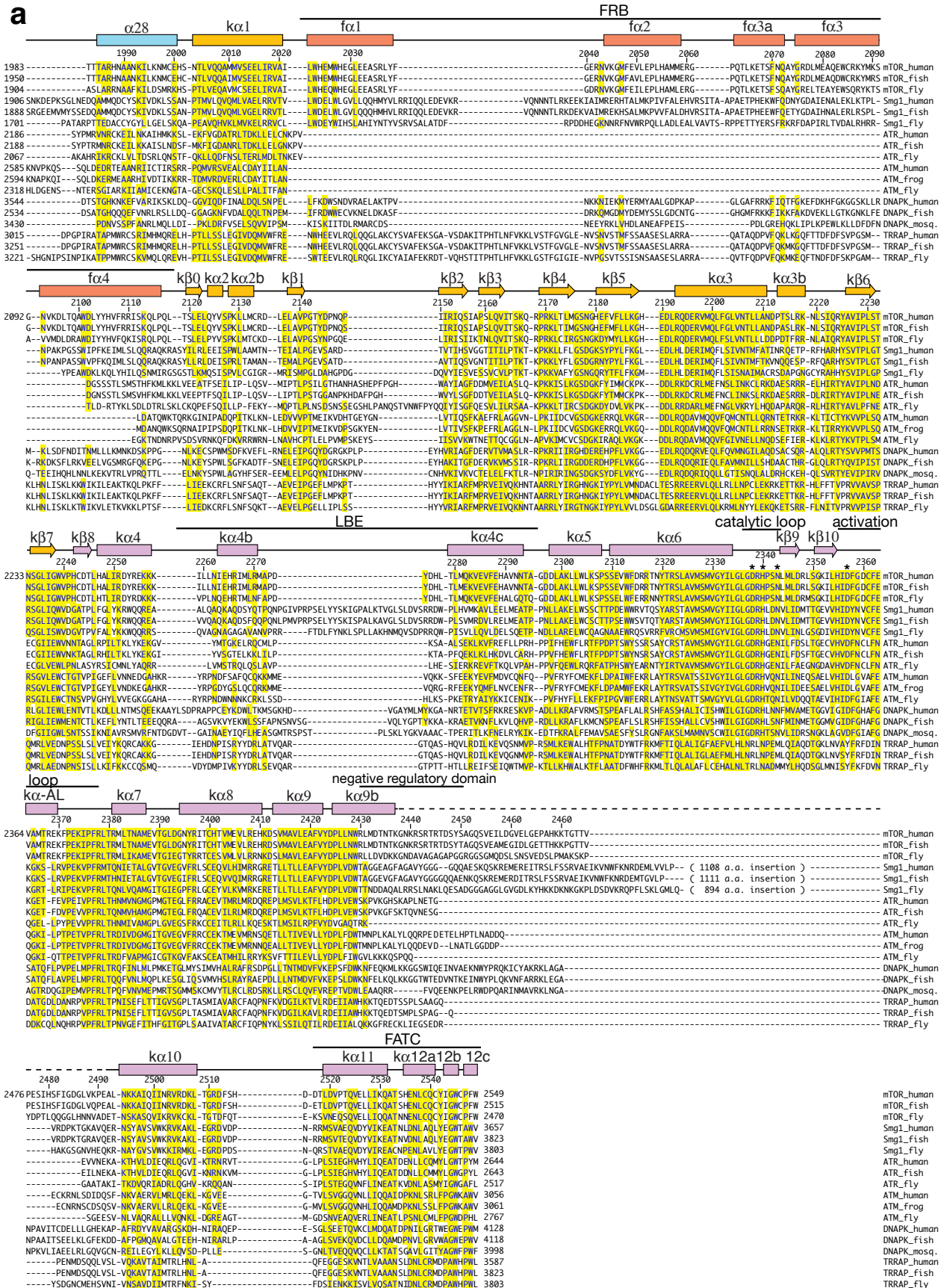
**Supplementary Figure 2. Secondary structure, sequence conservation and temperature factors of human mTOR<sup>AN</sup>.**

**a**, Sequences of human, fish, fly, budding yeast, fission yeast, plant and worm orthologs are shown. Helices are indicated as rounded cylinders,  $\beta$  strands as arrows, segments lacking regular secondary structure as solid lines, and disordered regions as dashed lines. The various domains are colored as in Figure 1a. The boundaries between the three TRD and one HRD domains are indicated by arrows. Segments discussed in text are indicated by horizontal brackets and are labeled. Active site residues

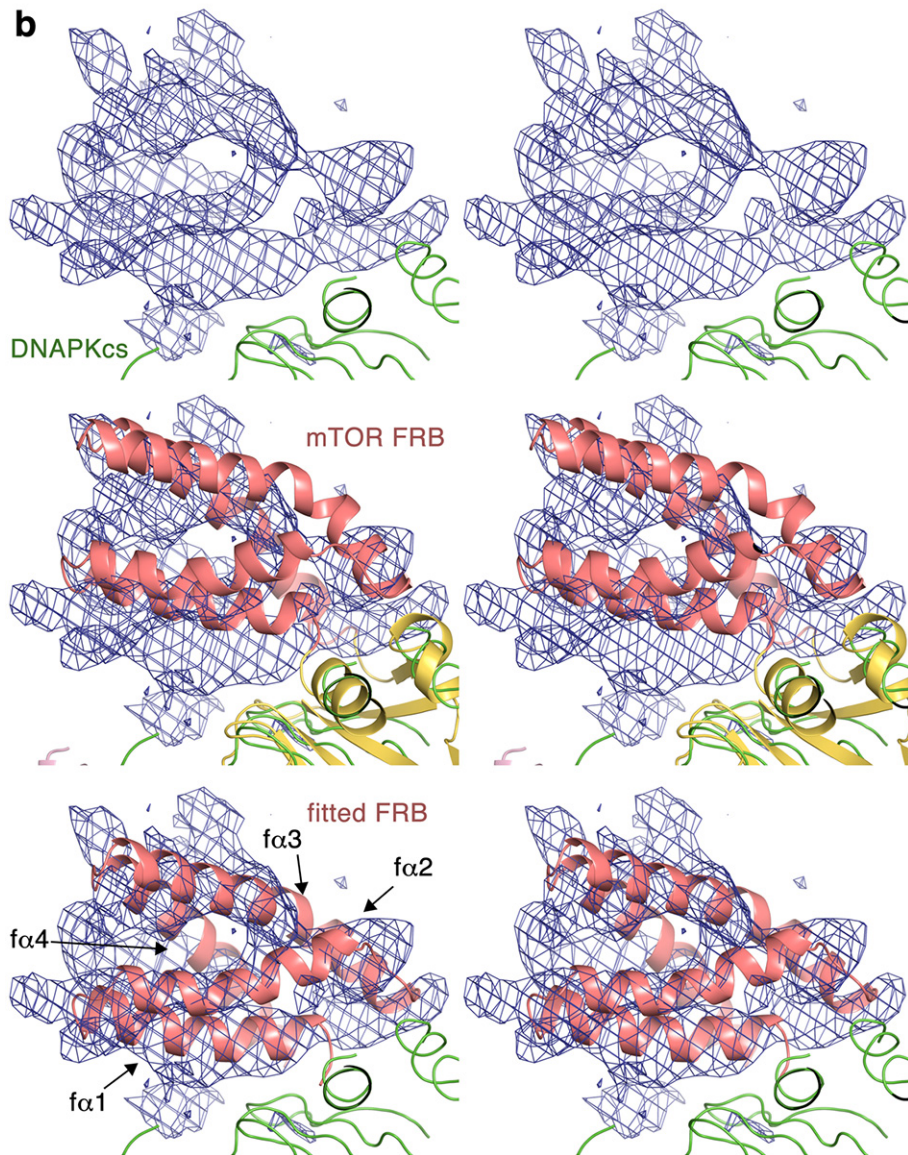
are marked by asterisks. The structure-based sequence alignment of the human PIK3C3, a type 3 PI3K (PDB 3IHY), is given as the last sequence extending across the kinase domain. The PIK3C3 residues that superimpose on mTOR are underlined, and dots represent insertions in the mTOR KD relative to PIK3C3.

**b**, Plot of the temperature factors (vertical axis of each panel in  $\text{\AA}^2$ ) of the mTOR<sup>ΔN</sup> C $\alpha$  atoms from one of the two mTOR<sup>ΔN</sup>-mLST8 complexes in the asymmetric unit of the apo crystals. The overall temperature factor of this entire mTOR<sup>ΔN</sup> protomer is 75.47  $\text{\AA}^2$  (92.60  $\text{\AA}^2$  for the second protomer), and of the kinase domain excluding the FRB is 50.44  $\text{\AA}^2$  (61.37  $\text{\AA}^2$  for the second protomer).

a







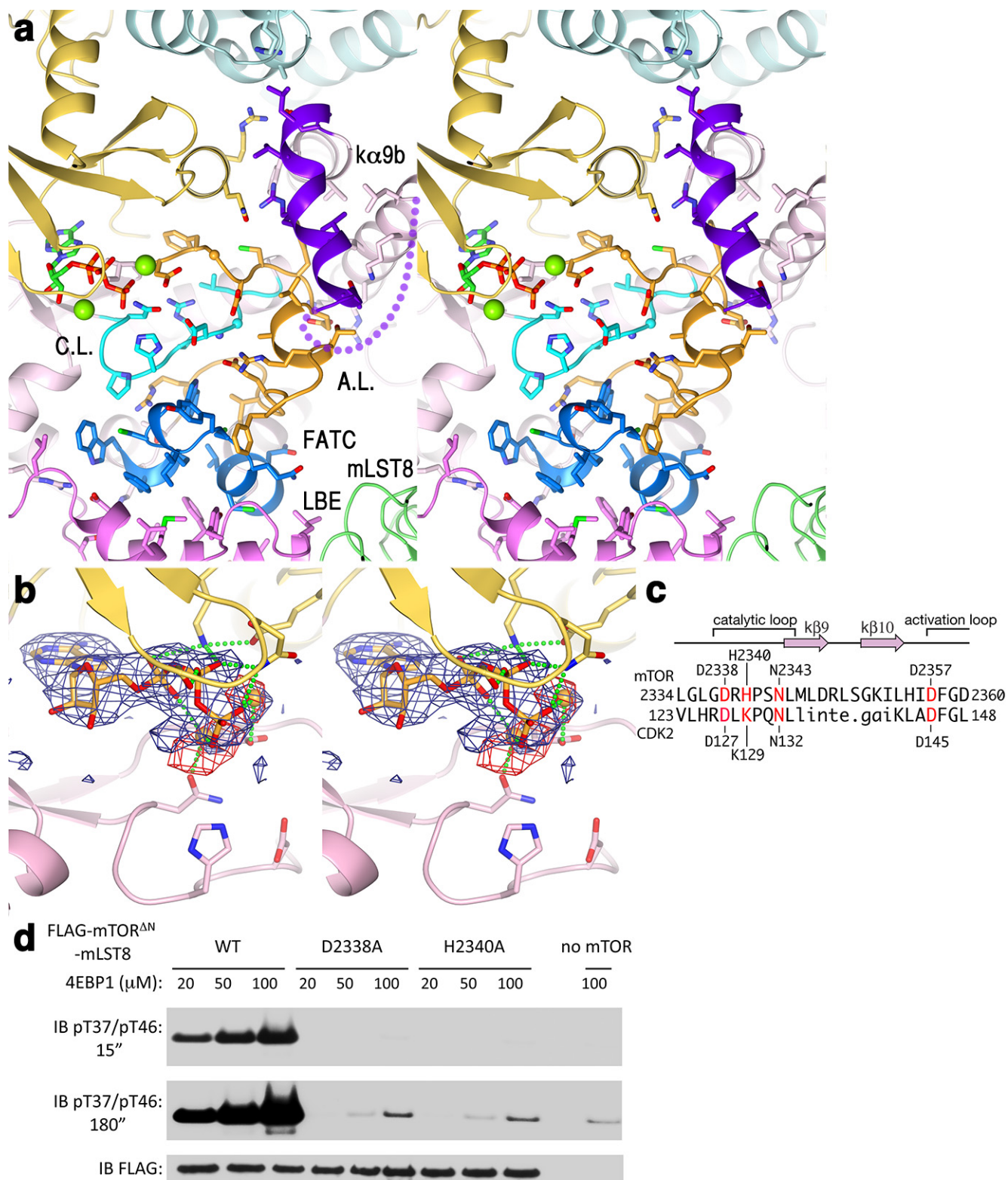
**Supplementary Figure 3. Comparison of the mTOR kinase domain to other PIKKs.**

**a**, PIKK sequence alignment of the KD region based on the mTOR structure. The FRB-like insertions in SMG1, DNAPKcs and TRRAP are predicted to be alpha helical by the JPRED server (<http://www.compbio.dundee.ac.uk/www-jpred/>). ATM and ATR appear to lack an insertion comparable to the FRB. The LBE-like insertions in all six PIKKs are predicted to have two helices, except for the longer insertion in SMG1. Secondary structure restraints from the mTOR structure were included in the alignment with the program Indonesia (<http://xray.bmc.uu.se/dennis/>). Annotations as in Supplementary Figure 2a. Residues with over 50 % sequence similarity are indicated in yellow.

**b**, An FRB-like domain is present in DNAPKcs. Top panel shows a stereo view of two-fold ncs averaged *F<sub>o</sub>-F<sub>c</sub>* electron density for the FRB region using the 6.6 Å native data of DNAPKcs<sup>1</sup> and phases from our rebuilding of the deposited model (PDB 3KGV). The deposited model, which lacks helices in the FRB region, is shown in green. Middle panel shows the superimposed mTOR structure, indicating that the FRB-like domain of DNAPKcs is tilted towards the C lobe. Bottom panel shows a manual fitting of the mTOR FRB (red) by optimizing the fit of helices f $\alpha$ 1 and f $\alpha$ 2 in the electron

density. Helices  $\alpha 3$  and  $\alpha 4$  appear to have different orientations compared to those of mTOR, which is expected given the sequence divergence between the two PIKKs. Figures were prepared with Pymol (The PyMOL Molecular Graphics System, Schrödinger, LLC).

We rebuilt the DNAPKcs model by first replacing the PI3K-based kinase domain in the deposited model with that of mTOR using molecular replacement and omitting the FRB, LBE and  $\alpha 9b$  to avoid model bias. Inspection of the resulting electron density maps revealed electron density consistent with the presence of all three omitted segments. In addition, the maps indicated that DNAPKcs should have essentially all 28 helices of the mTOR FAT domain, even though the deposited model contained only 17 helices in this region. The mTOR FAT domain was subsequently fitted into electron density that was calculated without any of the FAT helices, first as four rigid bodies corresponding to the TRD1, TRD2, TRD3 and HRD domains, then by adjustment of individual helical repeats (see Supplementary Fig. 13 for DNAPKcs FAT domain electron density and discussion). The resulting model was used to phase the *Fo-Fc* electron density shown.



**Supplementary Figure 4. The mTOR catalytic residues and reaction mechanism closely related to canonical protein kinases.**

**a**, Setero view of the spine of interactions (side chains within  $\sim 4$  Å distance) extending from the LBE (magenta) to the FATC (blue), activation loop (A.L. orange) and  $k\alpha 9b$  (purple) elements in the ATP $\gamma$ S

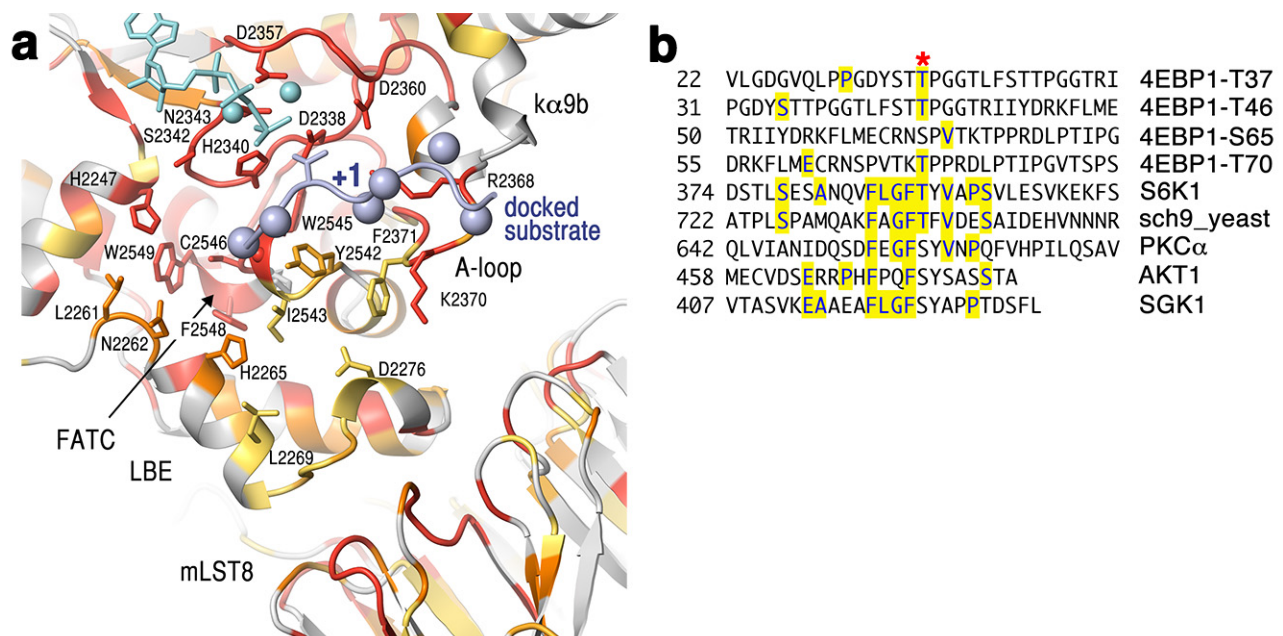
crystals. The catalytic loop (C.L.) is in cyan, and the remaining elements are colored as in Fig. 1a (light blue for FAT, yellow for N lobe, light pink for C lobe, and green for ATP $\gamma$ S). Purple dotted line indicates disordered loop between  $k\alpha 9b$  and  $k\alpha 10$ .

**b**, Stereo view of the *Fo-Fc* electron density of the ATP $\gamma$ S crystals, calculated at 3.3 Å and contoured at 2.5  $\sigma$ , is shown in blue mesh. Superimposed as red mesh is the anomalous fourier map of apo-crystals soaked in AMPPNP and manganese (Supplementary Table 1), after the map was skewed to the unit cell of the ATP $\gamma$ S crystals.

**c**, Structure-based sequence alignment of the catalytic and activation loop portions of mTOR and CDK2 that are superimposed in Figure 2c, with uppercase CDK2 residues having their C $\alpha$  atoms within 1.8 Å of the corresponding ones in mTOR (lowercase residues are displaced by 2.8 to 4.6 Å). The catalytic residues discussed in the main text are labeled and in red. We note that the mechanism proposed for PI3K postulated that a histidine (mTOR His2340) acts as the catalytic base, and an arginine (mTOR Arg2339) serves to neutralize the charge of the TS state. However, in mTOR the Arg2339 guanidinium group is  $\sim 7$  Å away from  $\gamma$ -phosphate TS mimic, compared to less than  $\sim 3$  Å for His2340, which we propose for this role. Furthermore, given that the relative arrangement of the Asp2338 catalytic base and the  $\gamma$ -phosphate TS mimic in CDK2 is nearly identical in mTOR, it is rather unlikely that this function will be carried out by a different residue in PIKKs or PI3Ks.

**d**, 4EBP1 phosphorylation by wild type, D2338A and H2340A FLAG-mTOR<sup>ΔN</sup>-mLST8, each at 100 nM concentration. Top panel is an immunoblot using an antibody specific for 4EBP1 phosphorylated at Thr37 and Thr46 and exposed for 15 seconds. Middle panel is the same immunoblot exposed for 180 seconds. Unphosphorylated 4EBP1 (no mTOR added) was run as a background control for the nonspecific signal from the antibody at long exposure times and at 100  $\mu$ M concentration of 4EBP1. From quantitation of multiple exposures we estimate the mutations reduce 4EBP1 phosphorylation by a factor of  $\sim 3000$  to  $\sim 9500$ . The bottom panel is an immunoblot with an anti-FLAG antibody.

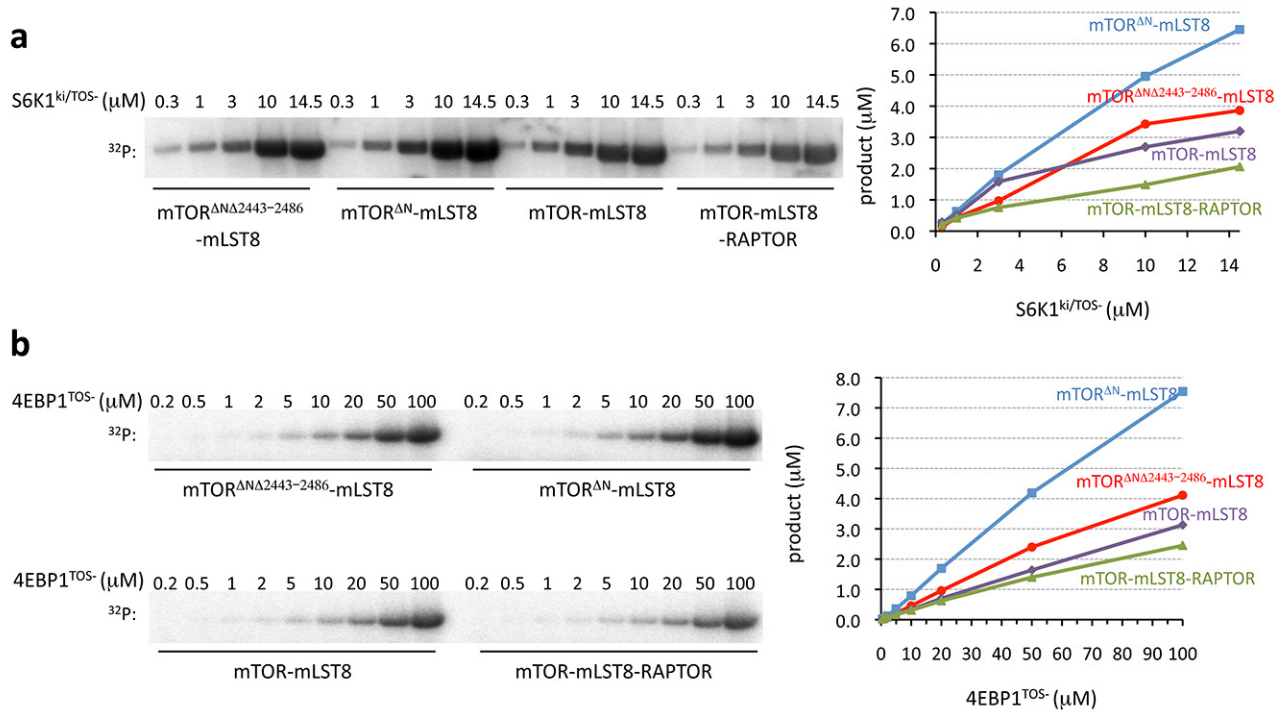
Supplementary Methods. The mutant and wild type (for direct comparison) complexes were produced by transiently transfecting 293-F cells with modified pcDNA 3.1 (+) vectors encoding FLAG-tagged wild type, D2338A or H2340A mTOR<sup>ΔN</sup> and untagged mLST8. After two days, the cells were harvested and the proteins were purified using anti-FLAG M2 agarose beads as described in Methods. After extensive washing of the beads, proteins were eluted with 0.1 mg ml<sup>-1</sup> FLAG peptide in 20 mM Tris-HCl, pH 8.0, 400 mM NaCl, 2 mM DTT, 10% glycerol, and concentrated. Protein concentrations were determined by A<sub>280</sub> and confirmed by immunoblotting with anti-FLAG antibody.



**Supplementary Figure 5. Putative substrate-binding grooves on the C lobe portion of the mTOR catalytic cleft.**

**a**, Stick representation of Figure 2d, showing the residues that line the putative substrate-binding groove on the C lobe portion of the catalytic cleft, colored by conservation as in Figure 2d (+1 position is labeled). In the (+) direction, the groove is lined by Phe2371, Tyr2542 and Trp2545, consistent with a positional scanning peptide array<sup>2</sup> showing preference for hydrophobic and aromatic residues at +1. In the (-) direction, there are multiple local pockets that extend farther away from the catalytic center. In addition to hydrophobic residues, there are several polar residues that are uninvolved in stabilizing the structure but are invariant in either all 22 orthologs (His2247) or in all but one (Asn2262 and His2265). These pockets could underlie the low-level of sequence preference at the -4 and -5 positions suggested by the positional scanning peptide array<sup>2</sup>.

**b**, Sequence alignments of the major phosphorylation sites (red asterisk) in the 4EBP1 and AGC kinase substrates of mTOR. Known mTOR substrates appear to lack a strong consensus motif at their phosphorylation sites. The four main phosphorylation sites of 4EBP1 have essentially no sequence homology flanking the Ser/Thr-Pro sites. While the ~7 residue HM motifs of the S6K1, AKT, PKC $\alpha$  and SGK1 AGC family kinases are conserved, they bear no relationship to the 4EBP1 sites. In addition, HM motif conservation is due, at least in part, to its role in mediating the activation of the kinase through phosphorylation-induced intra-molecular interactions<sup>3</sup>.



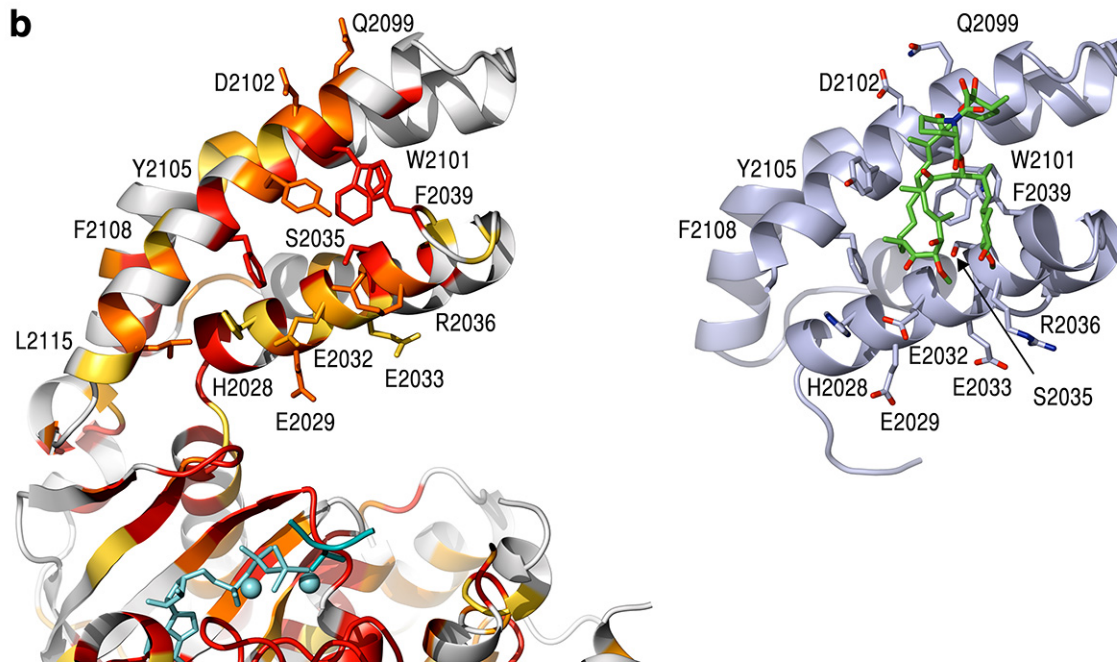
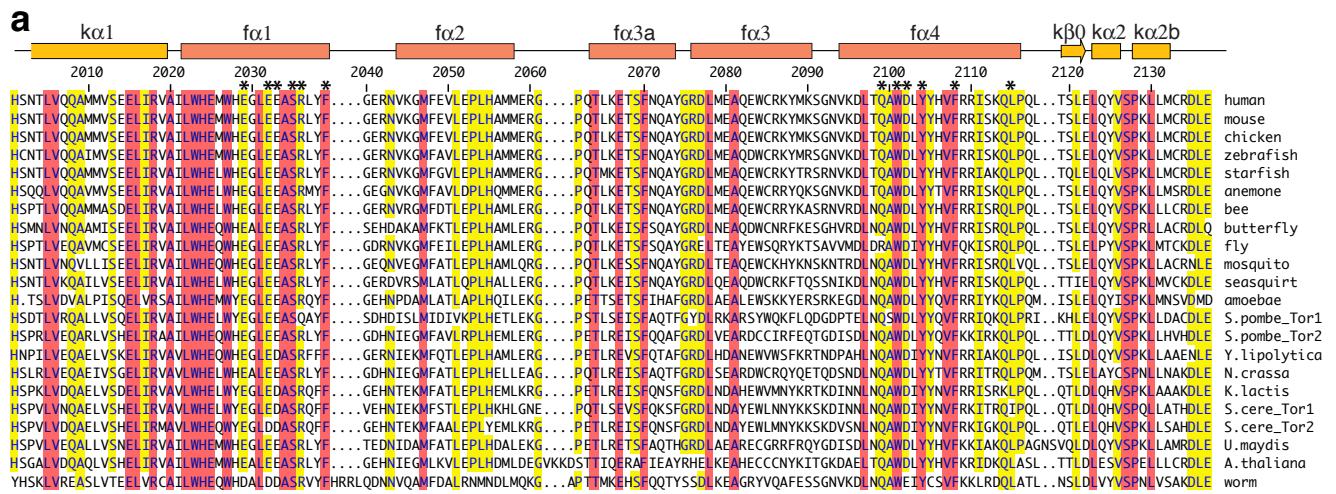
**Supplementary Figure 6. Comparison of the kinase activity of mTOR<sup>ΔN</sup>-mLST8, full-length mTOR-mLST8, mTOR-mLST8-RAPTOR, and mTOR<sup>Δ2443-2486</sup>-mLST8 complexes.**

**a**, Phosphorylation (<sup>32</sup>P autoradiogram) of the indicated concentrations of full-length S6K1<sup>ki</sup> with a mutated TOS motif (FDID to AAAA; S6K1<sup>ki/TOS-</sup>) by mTOR<sup>Δ2443-2486</sup>-mLST8 (red circles) mTOR<sup>ΔN</sup>-mLST8 (blue squares), mTOR-mLST8 (purple diamonds) and mTOR-mLST8-RAPTOR (green triangles), each at 100 nM concentration. Reactions were performed as described in methods. We do not understand the consistently lower kinase activity of mTOR<sup>Δ2443-2486</sup>-mLST8.

**b**, Phosphorylation (<sup>32</sup>P autoradiogram) of the indicated concentrations of full-length 4EBP1 with a mutated TOS motif (FEMDI to AAAAA; 4EBP1<sup>TOS-</sup>) by mTOR<sup>Δ2443-2486</sup>-mLST8 (red circles) mTOR<sup>ΔN</sup>-mLST8 (blue squares), mTOR-mLST8 (purple diamonds) and mTOR-mLST8-RAPTOR (green triangles), each at 100 nM concentration. Reactions were performed as described in methods.

Supplementary discussion of inhibition by rapamycin. In mTORC2, which is not inhibited by nanomolar rapamycin, there may not be enough space for rapamycin-FKBP12 to access the binding site on the FRB due to the proximity of other mTORC2 components. Consistent with the model that it is the FKBP12 component of rapamycin-FKBP12 that precludes binding to mTORC2, rapamycin can inhibit mTORC2 at micromolar concentrations, when it can bind to the FRB in the absence of FKBP12<sup>4</sup>. Also consistent with this model is the reduction in mTORC2 levels upon prolonged incubation with nanomolar rapamycin<sup>5</sup>, presumably because the de novo assembly of RICTOR with mTOR, which will now be bound to FKBP12-rapamycin, is blocked.

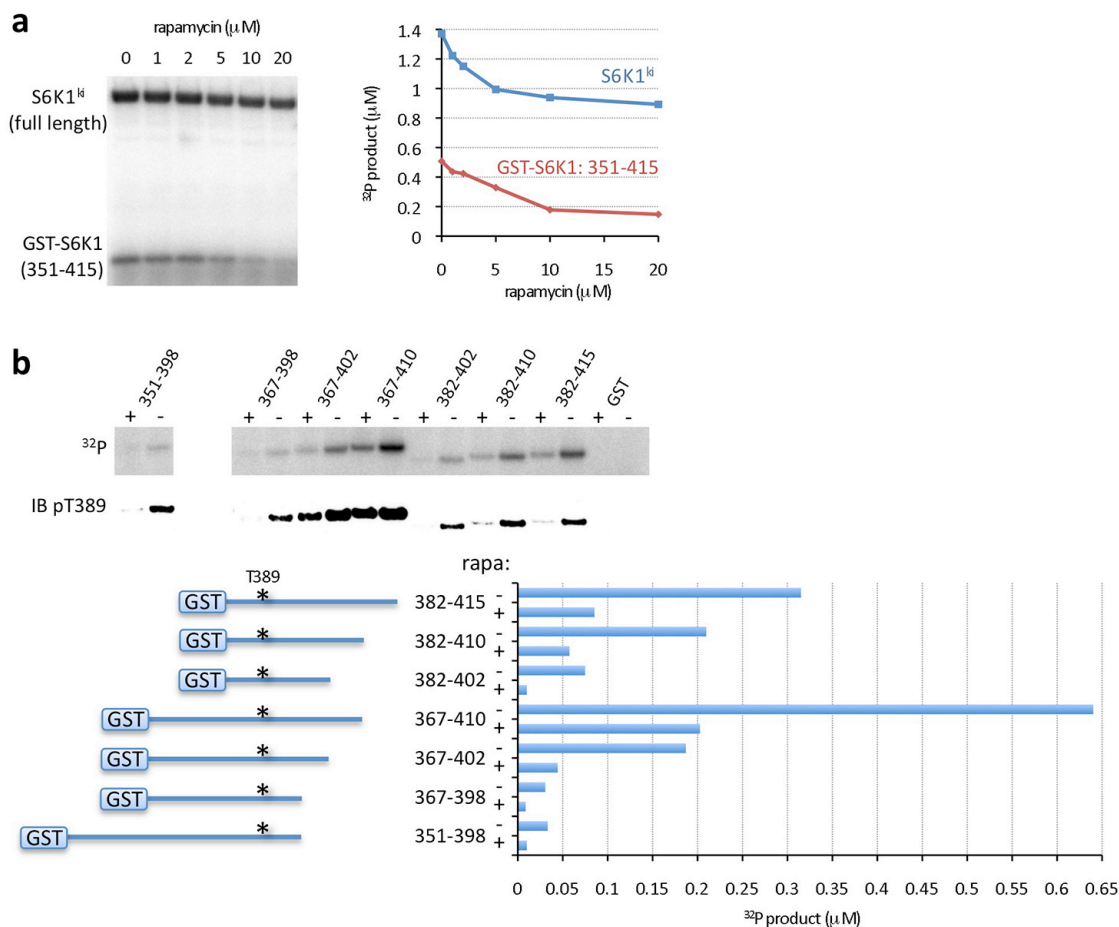
Prolonged rapamycin exposure can also destabilize the association of mTOR with RAPTOR<sup>6,7</sup>, as well as a dimeric arrangement of mTORC1<sup>8</sup>, although neither of these effects are observed with yeast TORC1<sup>9,10</sup>. It is conceivable that RAPTOR is close enough to the active site that there is barely enough space for FKBP12-rapamycin to fit in. Any residual steric hindrance may destabilize mTOR-RAPTOR during the binding equilibrium of the complex.



**Supplementary Figure 7.** The rapamycin-binding site maps to the FRB surface closest to the active site, in the midst of a hotspot of highly conserved residues.

**a**, Sequence conservation of the FRB in 22 mTOR orthologs and homologs (Tor2 in yeast), with 22/22 identity highlighted in red, and 19/22 in yellow. Residues that make up the conservation hotspot in and around the rapamycin binding site are marked by asterisks, and are shown in (b).

**b**, Left panel is a stick representation of figure 4a, showing the conserved residues in and around the rapamycin binding site. Right panel is the isolated FRB (light blue) bound to rapamycin (green) from the FRB-rapamycin-FKBP12 structure<sup>11</sup>.



**Supplementary Figure 8. Mapping of the S6K1 tail sequences required for the FRB-mediated recruitment to mTOR active site.**

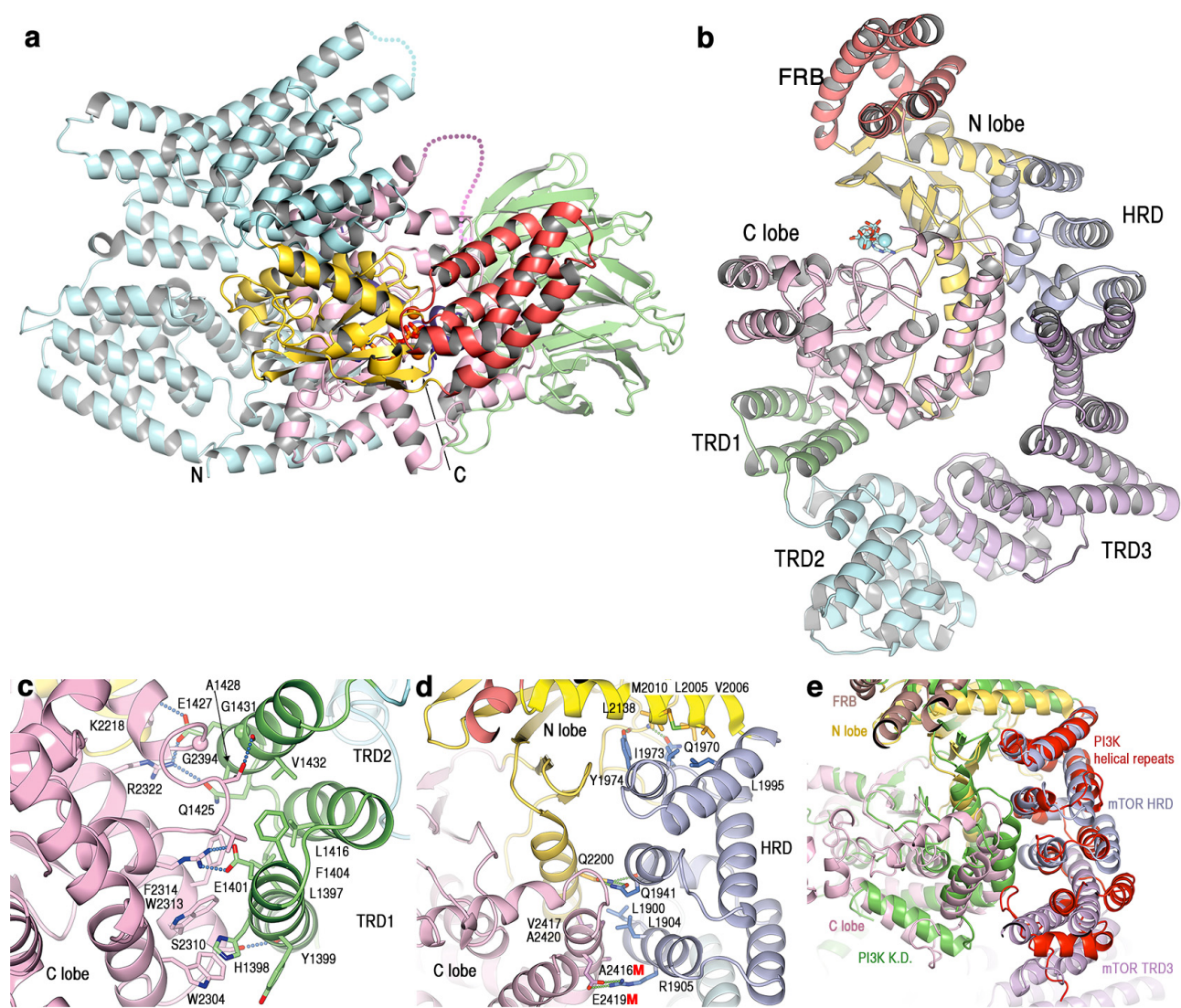
**a**, Inhibition, by the indicated concentrations of free rapamycin, of mTOR<sup>ΔN</sup>-mLST8 (100 nM) phosphorylation of full-length S6K1<sup>ki</sup> (blue squares) and a GST-tagged S6K1 polypeptide of residues 351-415 from the C-terminal tail (GST-S6K1<sup>351-415</sup>, red diamonds), each present at 2 μM concentration in the same reaction. Reactions were performed as in Methods. The S6K1 C-terminal tail, which starts with residue 351 immediately after the kinase domain structure<sup>12</sup> and ends at residue 502, is likely unstructured based on secondary-structure prediction programs (not shown). The reduced <sup>32</sup>P incorporation by GST-S6K1<sup>351-415</sup> compared to full length S6K1 is due, at least in part, to the presence of multiple in vitro phosphorylation sites after residue 416. Most of these sites are of unknown significance<sup>13,14</sup>.

**b**, Phosphorylation of the indicated GST-S6K1 tail polypeptides (2 μM) by mTOR<sup>ΔN</sup>-mLST8 (100 nM) and inhibition by free rapamycin (20 μM; lanes marked with +). Top panel is the <sup>32</sup>P autoradiogram, middle panel immunoblots using an S6K1 phosphoThr389-specific antibody, and bottom is <sup>32</sup>P quantitation. Reactions were performed as in Methods. C-terminal truncation of residues 403-410 reduces <sup>32</sup>P incorporation ~3-fold, while a further truncation of 399-402 results in an additional ~5-fold reduction, although phosphorylation remains rapamycin-sensitive. While N-terminal truncations of residues 367-381 reduce phosphorylation, this is caused by GST interference,



presumably due to its proximity to the HM motif when fused to residue 382, because the reduction is not observed after cleavage of the GST tag (not shown).

An alternative explanation for inhibition by free rapamycin and the dominant negative effect of the isolated FRB is that the FRB site mediates dimerization that may be important for substrate phosphorylation. Mammalian but not yeast TORC1 can form dimers, although this is dependent on RAPTOR, which is absent in our assays. Nevertheless, we found no evidence of mTOR<sup>ΔN</sup>-mLST8 dimerization or FRB binding to mTOR<sup>ΔN</sup>-mLST8. A hypothetical dimer whose inhibition by rapamycin or the isolated FRB would explain reduced S6K1 phosphorylation should be readily detectable, as it would have to form at mTOR<sup>ΔN</sup>-mLST8 concentrations as low as 20 nM used in the kinase assays of Figures 4b, c and d.



**Supplementary Figure 9. The FAT domain forms a C-shaped  $\alpha$  solenoid and clamps onto the kinase domain.**

**a**, Overall view of the mTOR<sup>ΔN</sup>-mLST8-ATP $\gamma$ S-Mg complex looking down the vertical axis of Figure 1, highlighting the C-shaped FAT domain clamping onto the KD. Colored as in Figure 1.

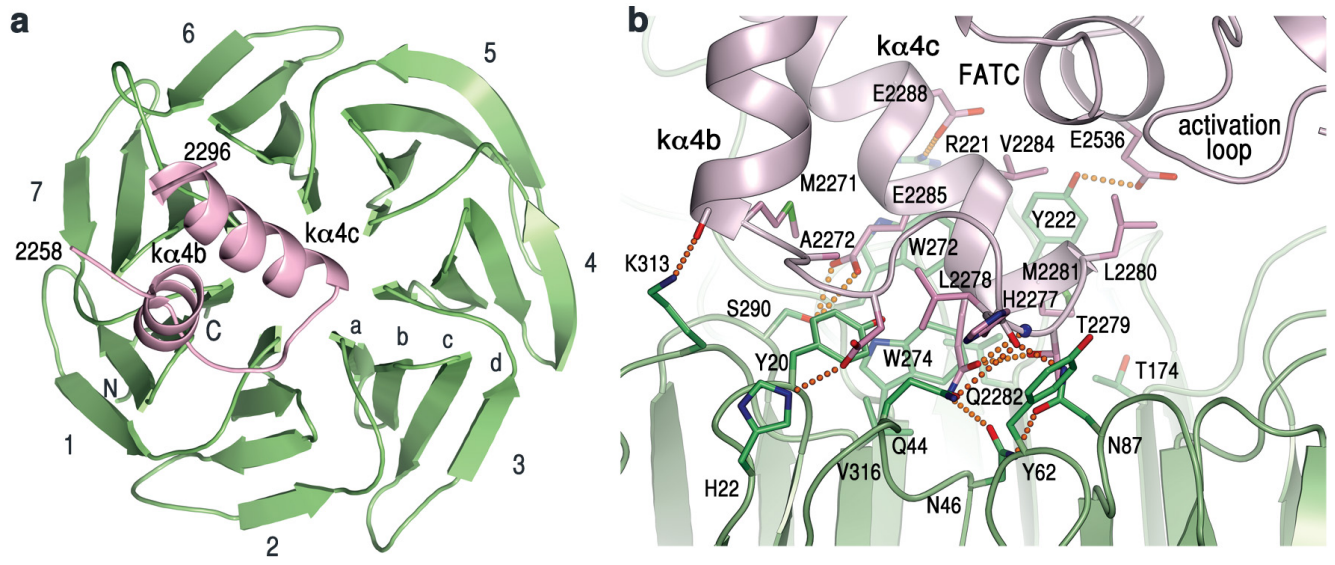
**b**, Overall view of mTOR<sup>ΔN</sup> with the FAT domain colored according to its three TPR domains and one HEAT repeat domain. TRD1 (light green) has 1.5 repeats, TRD2 (light cyan) has 4.5 repeats, TRD3 (light purple) has 5 repeats, and HRD (light blue) has 3 repeats. Based on the DALI server, TRD1 is structurally most similar to TPR repeats of Rab geranylgeranyltransferase- $\alpha$  (1LTX; Z-score 9.1); TRD2 to a synthetic consensus TPR protein (2HYZ; Z-score 13.5); TRD3 to the TPR-containing protein MamA (3ASH; Z-score 12.2), and HRD to the HEAT repeats of the microtubule binding protein XMAP215 (2QK2; Z-score 9.3) and the HEAT repeats of the PI3K p110 $\gamma$  (2V4L; Z-score 9.1). The non-canonical TRD1-TRD2 packing involves a lateral shift in the helical arrangement compared to regular TPRs, and it is stabilized by the TRD1  $\alpha$ 2 packing with the TRD2  $\alpha$ 11- $\alpha$ 12 loop. The TRD2-TRD3 packing is more divergent, being mediated by the second helix of TRD3 ( $\alpha$ 14) packing inside the concave surface of TRD2 ( $\alpha$ 6,  $\alpha$ 8,  $\alpha$ 10 and  $\alpha$ 12). This is associated with a reversal of

curvature between the two segments, and gives the TRD2-TRD3 portion of the  $\alpha$  solenoid a corkscrew-like twist. The HRD C-terminus forms a nearly continuous transition to the kinase N lobe, with only 2 amino acids intervening between the last HRD helix and the first KD helix.

**c**, Interface between TRD1 (green) and the KD C lobe (pink).

**d**, Interface between the HRD (light blue) and the KD C lobe (pink) and N lobe (yellow). The red letter “M” indicates two contact residues (Ala2416 and Glu2419) which were isolated as activating mutations of fission yeast Tor2p in the Rheb-independent growth screen<sup>15</sup>.

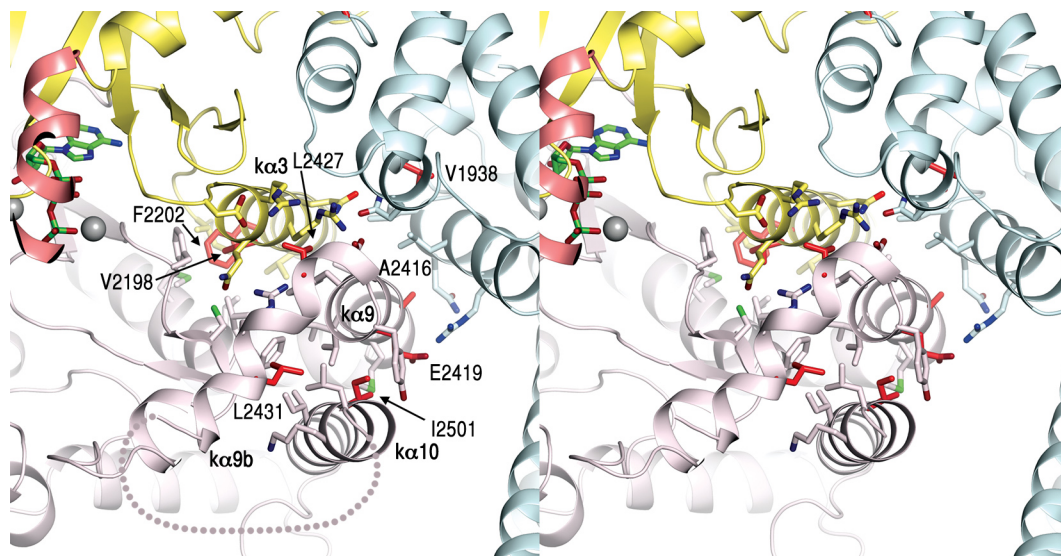
**e**, Superposition of the three HEAT repeats of the PI3K p110 $\alpha$  (PDB 2RDO) with the HRD (light blue) of mTOR. The p110 $\alpha$  HRD domain is in red and the rest of the protein in green. mTOR is colored as in (b), except the FRB is in brown. The mTOR HRD-KD contacts are also analogous to the p110 $\alpha$  HEAT repeat-KD contacts. For example, the mTOR Gln1941-Gln2200 interaction (Supplementary Fig. 9d) is also present in p110 $\alpha$  (Gln634-Gln815), and these residues are conserved in all PI3K family members. The rest of the FAT domain N-terminal to the HRD is unrelated to PI3Ks, which typically have at most two helical repeats capping the N-terminus of their HEAT-repeat domain.



**Supplementary Figure 10. mTOR-mLST8 interface.**

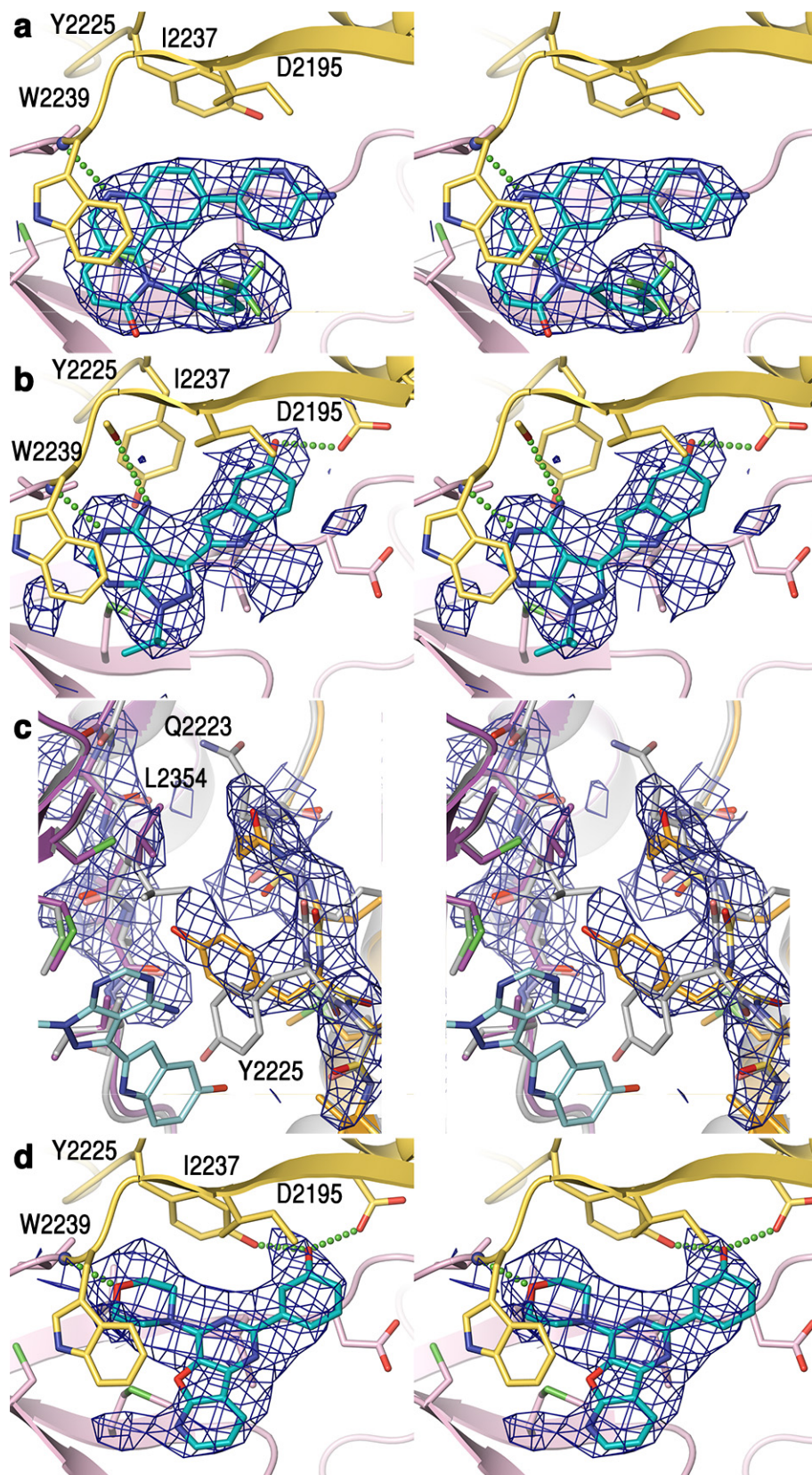
**a**, mLST8 (green) consists exclusively of seven WD40 repeats. They fold into a cononical  $\beta$  propeller structure, except for a permutation of the N- and C-terminal strands. The seven blades are numbered 1 through 7, and the strands of each blade are labeled “a” to “d”. Whereas in canonical WD40 domains the N-terminal strand corresponds to strand “d” of a blade (blade 7), the N-terminal strand of mLST8 corresponds to strand “b” (blade 1). Only residues 1-7 and 325-326 of the full-length mLST8 in the crystals are disordered. LBE (residues 2258-2296) is in pink.

**b**, The mTOR-mLST8 interface involves all but one of the mLST8 WD40 repeats, and both helices and intervening loop of the LBE, as well as a single residue from the FATC  $\alpha$ 12. View is rotated  $\sim 90^\circ$  along x from that of (a). In the absence of mLST8, there would be only two hydrophobic residues (Met2271 and Met2281) that would be solvent exposed on the LBE. These are unlikely to account for the reduced solubility (not shown) and heat-shock protein association<sup>16</sup> of mTOR overexpressed in the absence of mLST8.



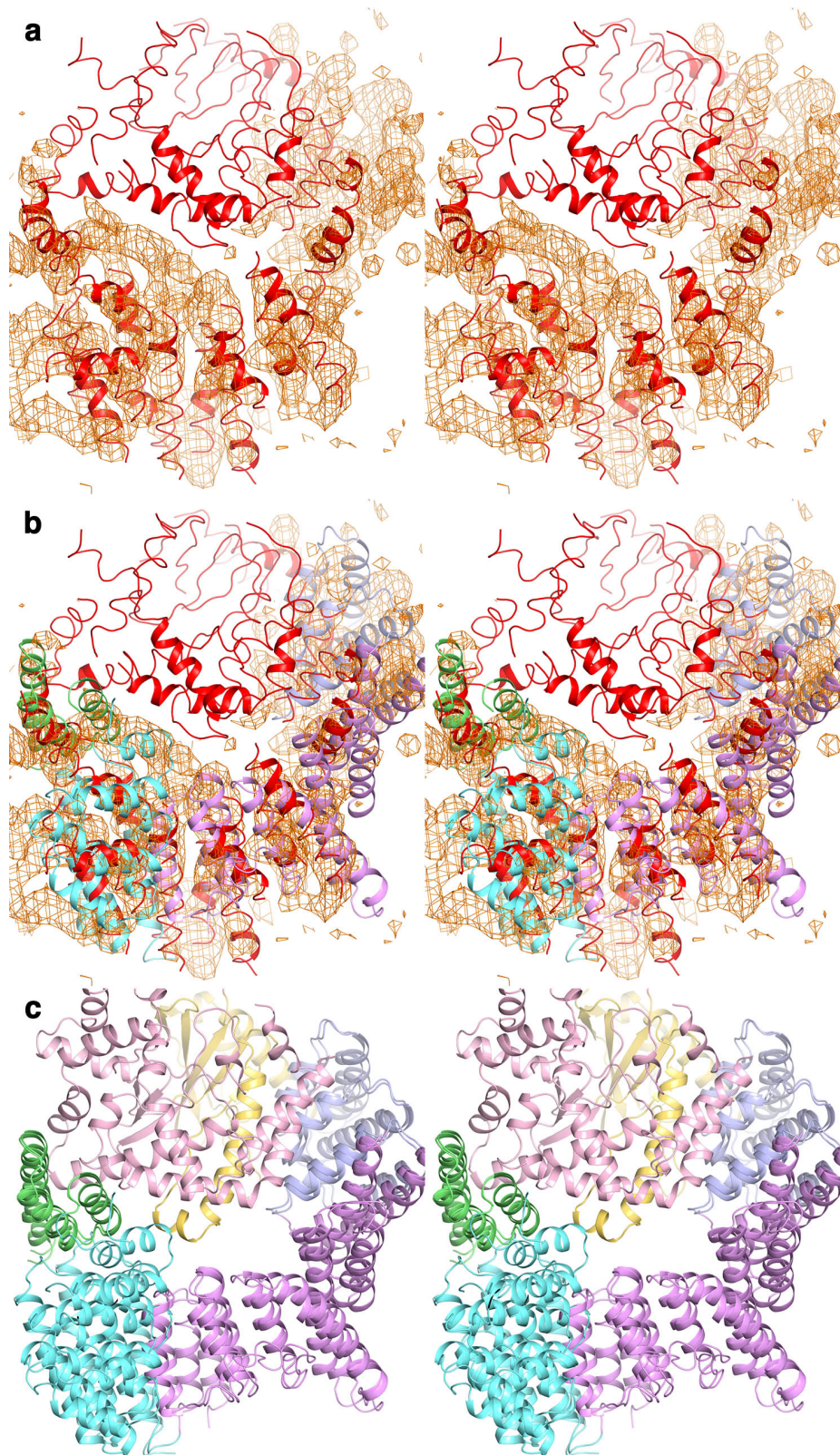
**Supplementary Figure 11. Close-up stereo view of activating mutations in the vicinity of  $\kappa\alpha 9b$ .**

Activating mutation residues at  $\kappa\alpha 9b$  or at the structural elements that pack with it ( $\kappa\alpha 3$ ,  $\kappa\alpha 9$  and  $\kappa\alpha 10$ ) are shown in red, and the residues in their immediate vicinity are shown in yellow (N lobe), pink (C lobe) or cyan (FAT HRD). Pink dotted line indicates the disordered loop between  $\kappa\alpha 9b$  and  $\kappa\alpha 10$ . The hyperactivating mutations were isolated in three separate screens for either bypassing the requirement for Rheb for growth<sup>15</sup>, suppressing the temperature-sensitive (ts) growth phenotype of an Lst8ts mutant<sup>17</sup>, or resistance to the ATP-competitive inhibitor caffeine. Figure 5 excludes three mutations that map to screen-specific structural elements. They are the A2290V and L2302Q mutations that map to the LBE and were isolated from the Lst8ts screen (discussed in the mLST8 section of the main text), and the ATP-site W2239R from the caffeine screen. The LBE A2290V and L2302Q mutations have not been assessed biochemically for increased mTOR phosphorylation activity, and the W2239R mutant is unlikely to be a general activating mutation; it has a temperature sensitive phenotype and the structure suggests it would have reduced affinity for both ATP and caffeine. Of the remaining mutations, only a subset has been assessed biochemically. However, the fact that Val2198 mutations were isolated in both the Rheb-null and Lst8ts screens is supportive of the notion that mutations that target the  $\kappa\alpha 9b$ -centered structural framework have a common effect in increasing mTOR kinase activity. We also note that while one of the mutant alleles from the Lst8ts screen (named SL1) has three mutations, we presume Val2198 is key for the hyperactive phenotype because the other two residues are not evolutionarily conserved.



Supplementary Figure 12. mTOR complexes with Torin2, PP242 and PI-103.

- a,** The 3.5 Å resolution *Fo-Fc* electron density of the Torin2–mTOR<sup>ΔN</sup>–mLST8 crystals, calculated with model phases before the inhibitor was built, is shown in stereo as a blue mesh contoured at 2.2 σ. View approximately looking down the vertical axis of Figure 6a. The N lobe portion of the cleft is above the plane of the figure, and it is not shown as it would obstruct the view. Green dotted line indicates atoms that are within hydrogen-bonding distance and geometry.
- b,** The 3.45 Å resolution *Fo-Fc* electron density of the PP242–mTOR<sup>ΔN</sup>–mLST8 crystals, calculated as in (a), and contoured at 2.2 σ.
- c,** Omit map of the two polypeptide segments from the N lobe (residues 2223-2226; orange) and C lobe (residues 2353-2355; pink) of the PP242–mTOR<sup>ΔN</sup>–mLST8 crystals that undergo a conformational change. The structure of the ATPγS-bound mTOR is in gray, and PP242 in light cyan. The 3.45 Å resolution *Fo-Fc* map was calculated with phases after the model with the omitted segments was subjected to simulated annealing refinement to remove model bias. Contoured at 2.0 σ.
- d,** The 3.6 Å resolution *Fo-Fc* electron density of the PI-103–mTOR<sup>ΔN</sup>–mLST8 crystals, calculated as in (a), and contoured at 2.2 σ.



**Supplementary Figure 13. DNAPKcs contains a FAT clamp that interacts with the KD domain as in the mTOR structure.**



**a**, Stereo view of two-fold ncs averaged *Fo-Fc* electron density for the FAT region using the 6.6 Å native data of DNAPKcs<sup>1</sup> and phases from our mTOR-based rebuilding (omitting the FAT) of the deposited model (PDB 3KGV). The deposited model, shown in red, contains only 17 of the 28 main mTOR FAT helices (2/3 helices in TRD1, 6/9 in TRD2, 7/10 in TRD3, and 2/6 in HRD). All but one ( $\alpha$ 20 of TRD3) of the missing helices are evident at the 2.5  $\sigma$  contour level shown.

**b**, Stereo view of the DNAPKcs FAT model constructed by fitting the mTOR TRD1, TRD2, TRD3 and HRD domains as rigid bodies into the density (colored as in Supplementary Fig. 8a). TRD1 and HRD require minimal adjustment consistent with their interactions with the KD. TRD2 and TRD3 are shifted and rotated substantially, consistent with their minimal sequence conservation among PIKKs. In addition, individual repeats of TRD2 and TRD3 and the last repeat of the HRD require additional shifts for fitting the electron density (not shown), and they also appear to differ in helix lengths compared to mTOR.

**c**, The mTOR<sup>AN</sup> structure superimposed on the rigid-body domain fitted FAT model of DNAPKcs, underscoring the similar arrangement of TRD1 and HRD relative to the KD, but divergent arrangements of TRD2 and TRD3.

## References

- 1 Sibanda, B. L., Chirgadze, D. Y. & Blundell, T. L. Crystal structure of DNA-PKcs reveals a large open-ring cradle comprised of HEAT repeats. *Nature* **463**, 118-121 (2010).
- 2 Hsu, P. P. *et al.* The mTOR-regulated phosphoproteome reveals a mechanism of mTORC1-mediated inhibition of growth factor signaling. *Science* **332**, 1317-1322 (2011).
- 3 Pearce, L. R., Komander, D. & Alessi, D. R. The nuts and bolts of AGC protein kinases. *Nat Rev Mol Cell Biol* **11**, 9-22 (2010).
- 4 Shor, B. *et al.* A new pharmacologic action of CCI-779 involves FKBP12-independent inhibition of mTOR kinase activity and profound repression of global protein synthesis. *Cancer Res* **68**, 2934-2943 (2008).
- 5 Sarbassov, D. D. *et al.* Prolonged rapamycin treatment inhibits mTORC2 assembly and Akt/PKB. *Mol Cell* **22**, 159-168 (2006).
- 6 Kim, D. H. *et al.* mTOR interacts with raptor to form a nutrient-sensitive complex that signals to the cell growth machinery. *Cell* **110**, 163-175 (2002).
- 7 Oshiro, N. *et al.* Dissociation of raptor from mTOR is a mechanism of rapamycin-induced inhibition of mTOR function. *Genes Cells* **9**, 359-366 (2004).
- 8 Yip, C. K., Murata, K., Walz, T., Sabatini, D. M. & Kang, S. A. Structure of the human mTOR complex I and its implications for rapamycin inhibition. *Mol Cell* **38**, 768-774 (2010).
- 9 Loewith, R. *et al.* Two TOR complexes, only one of which is rapamycin sensitive, have distinct roles in cell growth control. *Mol Cell* **10**, 457-468 (2002).
- 10 Adami, A., Garcia-Alvarez, B., Arias-Palomo, E., Barford, D. & Llorca, O. Structure of TOR and its complex with KOG1. *Mol Cell* **27**, 509-516 (2007).
- 11 Choi, J., Chen, J., Schreiber, S. L. & Clardy, J. Structure of the FKBP12-rapamycin complex interacting with the binding domain of human FRAP. *Science* **273**, 239-242 (1996).
- 12 Sunami, T. *et al.* Structural basis of human p70 ribosomal S6 kinase-1 regulation by activation loop phosphorylation. *J Biol Chem* **285**, 4587-4594 (2010).
- 13 McMahon, L. P., Choi, K. M., Lin, T. A., Abraham, R. T. & Lawrence, J. C., Jr. The rapamycin-binding domain governs substrate selectivity by the mammalian target of rapamycin. *Mol Cell Biol* **22**, 7428-7438 (2002).

- 14 Saitoh, M. *et al.* Regulation of an activated S6 kinase 1 variant reveals a novel mammalian target of rapamycin phosphorylation site. *J Biol Chem* **277**, 20104-20112 (2002).
- 15 Urano, J. *et al.* Point mutations in TOR confer Rheb-independent growth in fission yeast and nutrient-independent mammalian TOR signaling in mammalian cells. *Proc Natl Acad Sci U S A* **104**, 3514-3519 (2007).
- 16 Kim, D. H. *et al.* GbetaL, a positive regulator of the rapamycin-sensitive pathway required for the nutrient-sensitive interaction between raptor and mTOR. *Mol Cell* **11**, 895-904 (2003).
- 17 Ohne, Y. *et al.* Isolation of hyperactive mutants of mammalian target of rapamycin. *J Biol Chem* **283**, 31861-31870 (2008).